First-Order Scaling Law for Potential Vorticity Extraction due to Wind

BRUNO DEREMBLE AND W. K. DEWAR

Department of Earth, Ocean and Atmospheric Science, The Florida State University, Tallahassee, Florida

(Manuscript received 20 July 2011, in final form 19 April 2012)

ABSTRACT

Surface sources and sinks of potential vorticity (PV) have been examined recently in various publications. These are normally identified as the mechanical and buoyant PV fluxes with the former scaled according to wind stress and the latter from buoyancy flux. The authors here examine a PV source that is often overlooked: namely, the diabatically forced source due to wind-driven deepening.

Based on an idealized model of the mixed layer, the rate of deepening of the mixed layer due to wind is translated into PV extraction. The authors propose the first-order scaling law $J_z^W = (0.7f\rho u_*^3)/(gh^2)$ as an estimate of the net PV flux due to diabatic wind effects in the absence of other buoyancy effects. This law is verified and calibrated in several numerical experiments. Then, the authors compare the magnitude of the PV extraction due to wind to the other factors responsible for PV input/output: namely, air–sea heat flux, freshwater flux, and Ekman wind-driven currents. Finally, to illustrate the impact of the mixing induced by wind, the authors conclude with a global air–sea PV budget in the North Atlantic basin. The wind-driven diabatic PV flux is found to be comparable to all other sources in all cases and is distinguished by acting only to extract PV.

1. Introduction

Potential vorticity (PV) is a dynamic variable underpinning virtually all large-scale ocean theory (Pedlosky 1996) and has also proven useful in observational and diagnostic ocean studies (McDowell et al. 1982; Talley and Raymer 1982). It is thus of value to understand how PV enters the ocean and what the major sources and sinks of it are. An important contribution to this topic is due to Haynes and McIntyre (1987), who emphasized the general structure of PV, ending in the so-called impermeability theorem. Among other things, they showed that the sources of PV are at the surface of the ocean through interaction with the atmosphere and at the bottom of the ocean by means of interaction with the topography. It is of prime importance to have a good knowledge of these sources/sinks for a better understanding of ocean dynamics. Indeed, it has been shown that the formation of mode water is strongly affected by air–sea interaction [e.g., Marshall et al. (2009) for the subtropical mode water and Rintoul and England (2002) for the Antarctic Circumpolar Current (ACC)] and thus that its pronounced low PV signature is a result (Hanawa and Talley 2001).

Formulas for the boundary sources and sinks of PV have been developed (Marshall and Nurser 1992), and global estimates of them have been evaluated based on proposed scaling laws (Czaja and Hausmann 2009; Olsina et al. 2011, manuscript submitted to *Deep-Sea Res.*). At large scales, PV is well approximated by the product of the planetary vorticity and the vertical stratification,

$$Q_{\mathrm{qg}} = -\frac{f}{\rho}\frac{\partial \sigma}{\partial z}, \tag{1}$$

where f is planetary vorticity, σ is density[1] and $\partial\sigma/\partial z$ is the vertical stratification (Pedlosky 1996). The quantity ρ denotes a reference density. The minus sign is included to render PV positive in the Northern Hemisphere. From Eq. (1), it is clear that interactions tending to stratify the water column create PV, whereas vertical mixing in the water removes it. The two main atmospheric effects destroying PV are thought to be the following:

- Buoyant loss to the atmosphere (Warren 1972): The resulting convection mixes the oceanic upper layer

Corresponding author address: Bruno Deremble, The Florida State University, 117 N. Woodward Ave., Tallahassee, FL 32306-4320.
E-mail: bderemble@fsu.edu

DOI: 10.1175/JPO-D-11-0136.1

[1] By ''density,'' we mean potential density referred to the surface.

resulting in low PV. This can be driven by both heat and freshwater flux.

- Wind stress: Recently, it has been shown that in the presence of horizontal density fronts, Ekman currents driven by surface wind can drive dense water over light water, leading to convection and thus PV reduction (Marshall et al. 1993; Rintoul and England 2002; Thomas 2005; D'Asaro et al. 2011).

Scaling laws capturing these effects are the basis of the above-mentioned global studies.

It is also well known from mixed layer studies that the wind can drive mixed layer deepening, with attendant diabatic effects on surface density. This idea was present in the earliest of the so-called slab mixed layer models from the 1970s (see De Szoeke and Rhines 1976; Niiler and Krauss 1977; Cushman-Roisin 1981). In spite of its extensive history, however, the rate at which winds deepen the mixed layer remains open to debate. How much energy the winds add to the ocean is unclear (see, e.g., Sullivan and McWilliams 2010), as is the dissipation of mixed layer kinetic energy. It is nonetheless clear that the wind working on the ocean and surface turbulent dissipation acting in combination result in turbulent entrainment.

The main objective of the present study is to show that this mechanically driven form of convection is as important to surface PV fluxes as are buoyant convection and Ekman flux sources and that it is possibly larger than the latter. It is in this more detailed look at entrainment in an eddying model that we differ from Czaja and Hausmann (2009). In addition, as well as in contrast to these sources, which are not sign definite, wind-driven deepening can only reduce PV. Two of the key parameters expected to quantify this PV extraction are (i) the wind strength and (ii) the depth of the mixed layer. Based on numerical experiments, we provide a simple scaling law that measures the PV flux associated with mechanically driven convection by wind and use it to assess the relevance on PV flux of entrainment mixing.

The paper is organized as follows: After an introduction to the PV formalism, we propose the scaling law due to wind mixing in section 2. Then, we perform several idealized experiments to verify and calibrate this scaling in section 3. Finally, we use it in section 4 to quantify the PV extraction in the North Atlantic basin. We compare this term to the classical buoyancy and wind stress PV fluxes. Conclusions are given in section 5.

2. Scaling law

The impermeability theorem shows that PV can only move along density surfaces (Haynes and McIntyre 1987). Thus, it emphasizes that net oceanic PV can only be changed at outcrops (at the surface) or incrops (on topography).

a. PV formalism

The flux form of the PV equation is (see Marshall and Nurser 1992)

$$\frac{\partial}{\partial t}\rho Q + \nabla \cdot \mathbf{J} = 0, \tag{2}$$

where

$$Q = -\frac{1}{\rho}\boldsymbol{\omega} \cdot \nabla\sigma, \tag{3}$$

with $\boldsymbol{\omega}$ being the total vorticity, the sum of the planetary and relative vorticity,

$$\boldsymbol{\omega} = f\mathbf{k} + \nabla \times \mathbf{u}; \tag{4}$$

σ being the potential density; and ρ being a reference density.

One can write $\mathbf{J}$ in several ways (Marshall et al. 2001). Usually, one refers to $\mathbf{J}$ as the sum of advective and non advective parts,

$$\mathbf{J} = \rho Q\mathbf{u} + \boldsymbol{\omega}\frac{D\sigma}{Dt} + \mathbf{F} \times \nabla\sigma + \frac{\Phi}{\rho_o}\nabla\rho \times \nabla\sigma, \tag{5}$$

where $\mathbf{F}$ is the nonconservative forces of the momentum equation. In the following, we refer to the second term, $\boldsymbol{\omega}D\sigma/Dt$, as the buoyancy term and the third term, $\mathbf{F} \times \nabla\sigma$, as the mechanical term. The main air–sea exchanges acting on PV are net heat flux $Q_{\rm net}$ and wind stress. Scalings for the primary means by which these exchanges create PV have been suggested in Thomas (2005), specifically the vertical component of both the buoyancy and mechanical terms of the $\mathbf{J}$ vector, are

$$J_z^B = -\frac{f\alpha Q_{\rm net}}{hc_p} + \frac{f\beta S(E-P)}{h} \tag{6}$$

and

$$J_z^F = \frac{\boldsymbol{\tau} \times \nabla\sigma}{\rho\delta_e}, \tag{7}$$

where α and β are the thermal and haline expansion coefficients, h is the depth of the mixed layer, c_p is the specific heat capacity, S is the surface salinity, $(E - P)$ is the freshwater flux, $\boldsymbol{\tau}$ is the surface wind stress, and δ_e is the depth of the Ekman layer. This depth is usually approximated by $\delta_e = 0.4u_*/f$, with $u_* = \sqrt{|\boldsymbol{\tau}|/\rho}$.

Equation (7) captures the powerful PV creation mechanics driven by winds oriented in the down-front direction recently discussed by Thomas (2005). We argue here that the wind is not only an active agent of PV production/destruction in regions of strong SST fronts but also from wind-driven mixed layer deepening. To do so requires the wind to be active through the buoyancy term as well as the mechanical term.

b. Scaling for the PV flux in the absence of heat flux

The idealized vertical density profile in Fig. 1 can be divided in three parts: the mixed layer of thickness h, a zone of rapid density variation (here shown as a discontinuity), and the ocean interior with a slowly varying density. The density jump between the mixed layer and the ocean interior is denoted as $\Delta\sigma$. The potential energy per unit area relative to the fluid under the mixed layer is given by

$$E_p = \frac{g'h^2}{2}, \tag{8}$$

where $g' = g\Delta\sigma/\rho$ is the reduced gravity.

Classical arguments lead to scalings for the rate of wind work on the ocean like

$$E_K^t \sim u_*^3, \tag{9}$$

where u_* is the friction velocity (Cushman-Roisin 1981). Ultimately, this powers up the wind-driven component of the circulation, although the pathways by which this occurs are not clear (Alford 2003a). Wunsch and Ferrari (2004) (see their Fig. 5 in particular) emphasize this point and argue that something like half of the wind input is locally dissipated in the surface and that half drives ocean currents. Some fraction of that dissipated manifests as potential energy gain in the mixed layer. The form of the scaling appearing in Eq. (9) has been supported recently in Gerbi et al. (2009) and Sullivan and McWilliams (2010), although both argue the premultiplier is large [O(10–100)] and depends upon wave age and sea state (see also Terray et al. 1996). We assume here that a standard fraction λ of the wind working is converted into potential energy (this assumption is tested in the next section). By equating the rate of variation of potential energy [dEq. (8)/dt] and the input of energy [Eq. (9)], one obtains

$$g'h\frac{dh}{dt} = \lambda u_*^3. \tag{10}$$

The parameter λ remains to be specified. This equation is similar to those appearing in early slab mixed layer models (Pollard et al. 1972; Cushman-Roisin 1981; Price et al. 1986). The simple form of the above equation should be contrasted with the nature of surface dissipation, which involves complex phenomena like breaking waves (Thorpe et al. 2003; Gerbi et al. 2009), turbulence, convection, and Langmuir circulation (Smith 1998, 2001; Thorpe 2004). Li et al. (2005) provide a description of the different regimes that occur for varying surface stress and surface buoyancy forcing. Grant and Belcher (2011) discuss the energy budget in and below the mixed layer with an emphasis on shear mixing at the mixed layer base, and Alford (2003a,b) emphasizes the role of nonlocal effects. In spite of these complexities, we are motivated to test the above simple relationship for the purposes of assessing the significance of entrainment to PV flux.

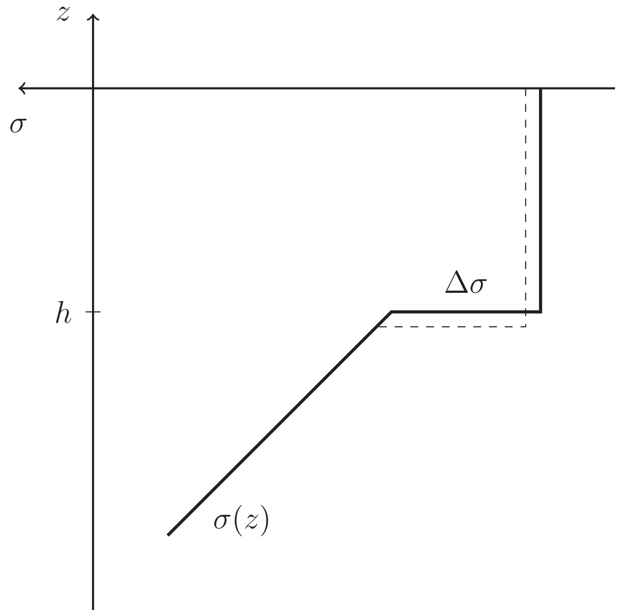

FIG. 1. Schematic view of the density profile in the upper ocean: the mixed layer of thickness h (constant density profile) and the ocean interior (density slowly decreasing with depth) are separated by the thermocline (rapid variation of the density $\Delta\sigma$). The dashed line mimics the evolution of the density profile because of mixing in the mixed layer and erosion of the thermocline.

We are interested in the variation of σ when the mixed layer depth increases. In the absence of surface buoyancy flux, the density equation in the mixed layer reduces to (see also Fig. 1):

$$\frac{d\sigma}{dt} = \frac{\Delta\sigma}{h}\frac{dh}{dt}. \tag{11}$$

Combining Eqs. (10) and (11) to estimate the rate of variation of the density, a scaling law for the extraction of PV due to wind by mixing processes is obtained. Using planetary vorticity f to estimate $\boldsymbol{\omega}$, we have

$$J_z^W = \lambda\frac{f\rho u_*^3}{gh^2}. \tag{12}$$

c. Discussion

Our plan is to estimate a value for λ in Eq. (10) by experimentation with the Massachusetts Institute of Technology General Circulation Model (MITgcm) ocean general circulation model (Marshall et al. 1997). Although possible, our plan is not to perform large-eddy simulations (LES) per se to accomplish this; rather, we will employ the MITgcm using the well-known *K*-profile parameterization (KPP) (Large et al. 1994). The latter models all surface phenomena in the form of vertically and temporally variable coefficients of viscosity and diffusivity.

LESs of the surface layer have been the object of several previous studies (e.g., Skyllingstad and Denbo 1995; McWilliams et al. 1997; Skyllingstad et al. 2000). Support for KPP can be found in several studies, such as the LES of Harcourt and D'Asaro (2008). Large and Gent (1999) argue a favorable comparison between KPP and LES under wind and buoyancy forcings. McWilliams and Sullivan (2000) proposed a modification to KPP to account for Langmuir circulations. Smyth et al. (2002) review these revisions, propose modifications to account for differing sea states, and find that comparable mixed layer depths are obtained by KPP relative to an LES in spite of discrepancies in temperature and momentum gradients. Sullivan and McWilliams (2010) test KPP against an LES under wind and convective forcing and find accurate performance.

Last, KPP has been verified in several oceanic general circulation model settings (Large et al. 1994; Large and Gent 1999; Li et al. 2001). Bernie et al. (2005) successfully compare KPP predictions against the Tropical Ocean and Global Atmosphere Coupled Ocean–Atmosphere Response Experiment (TOGA COARE), provided high spatial (1 m) and temporal (1 h) resolution is used. Wijesekera et al. (2003) and Durski et al. (2004) find good agreement between KPP and turbulence closure models in the coastal regime.

In summary, KPP provides an accurate, if parameterized, view of mixed layer evolution. We therefore use it to estimate the connection between wind working on the ocean and potential energy development in the mixed layer due to entrainment at the mixed layer base.

3. Idealized experiment

a. Description

We deploy the MITgcm in a 5 km × 5 km × 1000 m domain with 1-km resolution in x and y and 160 vertical levels. Periodic boundary conditions are used in the horizontal. The vertical discretization is 2 m for the first 100 m, 5 m for the next 200 m, and 10 m for the last 700 m. The fluid is initially at rest. The initial conditions for the temperature and salinity are independent of horizontal position, thus avoiding surface density gradients that would otherwise generate PV via the third term in Eq. (5). Vertical profiles from (36°N, 45°W) in the North Atlantic are obtained from the first half of 2006 from the Hybrid Coordinate Ocean Model (HYCOM) reanalysis dataset (Chassignet et al. 2007) in order to see the impact of the summer/winter contrast in mixed layer structure. We retain one vertical profile every 15 days (starting on 1 January 2006). The base of the mixed layer is the depth at which the temperature has changed by 0.8 K with respect to the surface temperature (see also the discussion in Kara et al. 2000). The background viscosity values are $\nu_h = 50\ \mathrm{m^2\ s^{-1}}$ and $\nu_v = 10^{-5}\ \mathrm{m^2\ s^{-1}}$ in the horizontal and vertical directions, respectively, although the KPP model modifies the effective viscosity from the background based on surface conditions.

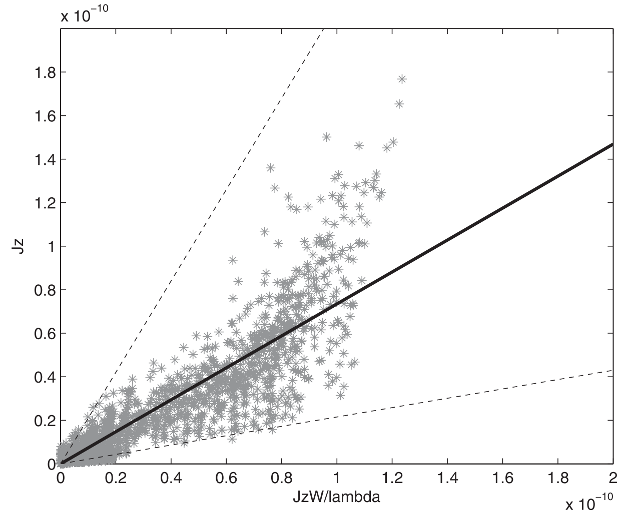

FIG. 2. Plot of J_z computed using Eq. (5) vs J_z^W/λ computed using Eq. (12). Each dot corresponds to a particular simulation with a given temperature and salinity profile. The thick line is a standard linear regression, and the two dashed lines link the extreme values.

The model is first integrated without any surface forcing. In that configuration, the PV flux at the surface is zero, as expected. Then, the ocean is forced by a surface wind. For each temperature and salinity profile, we use various winds ranging between 5 and 20 m s^{-1} (with a sampling of 1 m s^{-1}). The model is integrated for 3 days, of which we analyze the last 2 days.

b. Estimate of λ

Figure 2 is the main result of the experiment described above. We plot the vertical component of the **J** vector computed using the full formulation [Eq. (5)] versus the scaling [Eq. (12)]. A standard linear regression to these data gives $\lambda = 0.7$.

The scatter about the fit reminds us that mixed layer deepening is a complex process only very crudely captured by our approach. The value of the slope linking the minimum J_z values to the origin gives $\lambda_{\min} = 0.21$, whereas the slope of the curve linking the origin to the maximum J_z yields $\lambda_{\max} = 2.1$. These two curves are plotted with dashed lines in Fig. 2. We claim that the fit is skilled because the extreme slopes of the regression do not exceed one order of magnitude. The correlation between the scaling law and the model results is 0.73 and is significant at the 95% level. When plotting the rate of variation of the potential energy as a function of the input energy, we obtain a similar value of λ (not shown). Higher winds lead to greater ensemble dispersion, suggesting the linear hypothesis mentioned above might not be valid for winds above 20 m s^{-1}.

It is useful to compare our inferred relation with other more detailed estimates. For example, one infers from Fig. 17 in Grant and Belcher (2011) a deepening of 0.12 m h^{-1} for a mixed layer forced by a constant wind stress of 0.037 N m^{-2} ($\simeq$6 m s^{-1}). Adopting their mixed layer temperature jump ($\Delta T = 0.1$ K; see their Fig. 3) and $h = 25$ m, $u_*^3/g'h = 0.15$ m h^{-1}, which returns $\lambda \simeq 1$.

Based on law of the wall reasoning (Agrawal et al. 1992; Terray et al. 1996), Gerbi et al. (2009) argue for a lower bound mixed layer turbulent dissipation rate corresponding roughly to $\lambda = 0.1$. This number depends on surface waves (Agrawal et al. 1992) and wave frequency (Terray et al. 1996).

The observations in Smith (1998) suggest a deepening of 3 m h^{-1} under a wind of 13 m s^{-1} for a 20-m mixed layer with temperature step $\Delta T = 0.1$ K. We obtain in this case a value of $u_*^3/g'h = 2$ m h^{-1}, again implying an $O(1)$ value for λ, here in the regime for which the scatter in Fig. 2 increases. Other studies also suggest a deepening rate of 3 m h^{-1} for the same wind conditions (e.g., D'Asaro 2001). In summary, our inferred value of $\lambda \sim 0.7$ yields deepening rates that compare well to both direct observations and detailed mixed layer models.

c. *Estimate of λ in the presence of heat flux*

If buoyancy fluxes are present, as they almost always are, the arguments in section 2 require some modification. The simple situation is that of wintertime buoyancy loss, which provides an additional energy source for homogenizing mixed layer density. We suggest in this case wind-driven entrainment will proceed according to the above formula, at least at leading order (for cautionary statements, however, see Li et al. 2005).

The summertime is different because of the addition of buoyancy to the surface layer, thereby presenting the wind input with a potential energy barrier that must be overcome prior to the wind-driven entrainment of any sub–mixed layer waters. If the rate of potential energy injection into the surface exceeds the ability of the wind to mix, no entrainment will occur. This energy barrier is given by

$$\Delta E = -\frac{\alpha Q_{\text{net}} h}{c_p} + \beta S(E - P)h + \lambda \frac{\rho u_*^3}{g}. \qquad (13)$$

To illustrate the summer/winter contrast, the previous experiment has been modified to include a heat flux. We now measure the PV extraction (or input) when the wind and heat flux act jointly (Fig. 3). For this new experiment, we select a subset of density profiles/wind stress from the previous experiment. The heat flux values tested are -200, -100, 100, and 200 W m^{-2}, which are typical of observed heat fluxes.[2]

In Fig. 3, the y axis is $J - J_z^B$ while the x axis is still J_z^W/λ. Figures 3a,b show that the value of $\lambda = 0.7$ found previously is an overestimation when the ocean is heated. A standard linear regression gives values of 0.63 (Fig. 3a) and 0.69 (Fig. 3b) for λ.

Figures 3c,d show the opposite tendency: the previous scaling underestimates the extraction of PV. A linear regression gives values of $\lambda = 0.85$ (Fig. 3c) and $\lambda = 0.91$ (Fig. 3d).

From Fig. 3, we conclude that $\lambda = 0.7$ is a reasonable approximation across a variety of conditions even for relatively strong cooling or heating. For larger values of heat flux the additive rule $J = J_z^B + J_z^W$ might no longer be valid (the wind and heat flux can combine in a nonlinear way to modify the density profile of the mixed layer).

Figure 6 in Price et al. (1986) provides a good illustration of the competition between the wind and the surface heat flux during a diurnal cycle. During the day, the heat flux drives a restratification of the water column. However, as shown in Price et al. (1986), such restratification occurred only 1 day out of 4, when the magnitude of the wind stress was small (less than 0.02 N m^{-2}). On the other days, the wind stresses, between 0.1 and 0.2 N m^{-2}, were sufficient to prevent diurnal restratification.

4. Mapping in a realistic case

We now use this scaling to quantify the relative importance of this effect in the North Atlantic. To simultaneously

[2] The monthly-mean heat flux varies from -150 W m^{-2} in summer to 150 W m^{-2} in winter at a standard location in the ocean; this range shifts to -100 W m^{-2} in summer to 600 W m^{-2} in winter over the western boundary currents.

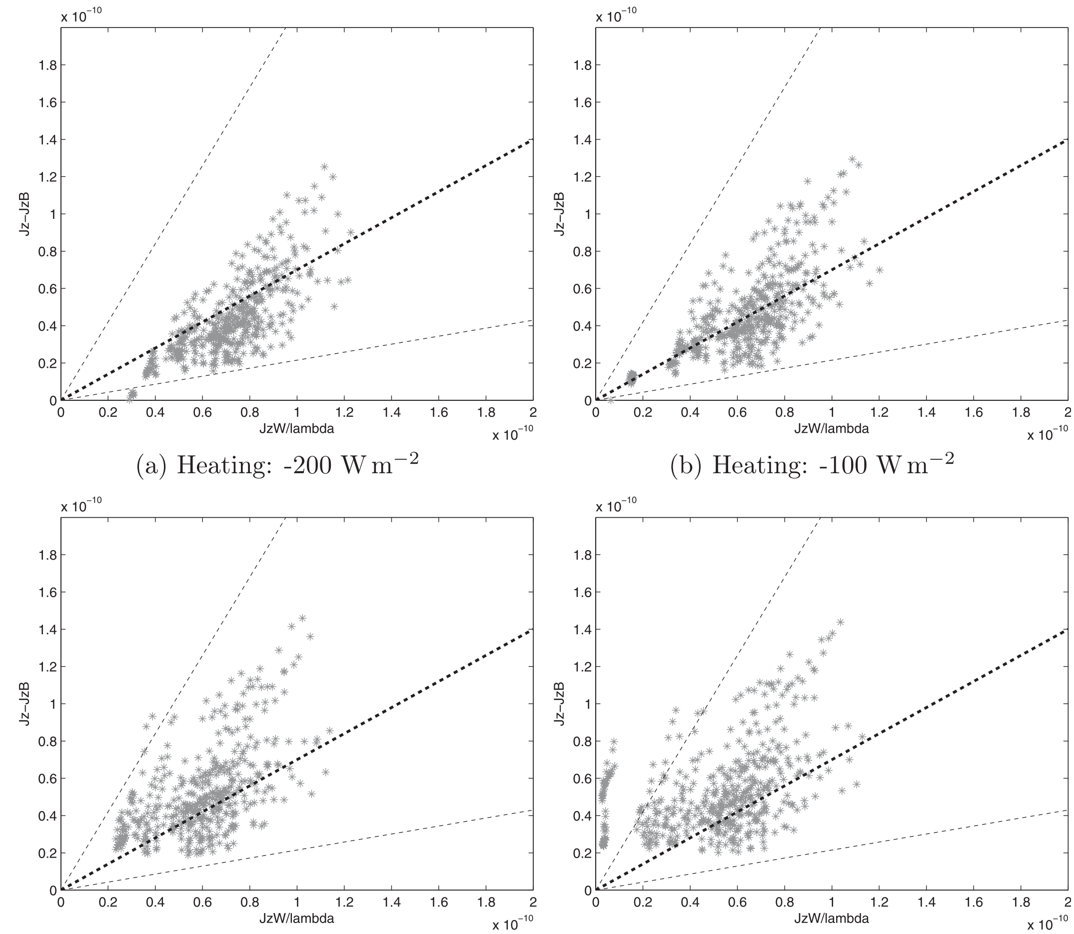

(a) Heating: -200 W m^{-2} (b) Heating: -100 W m^{-2}

(c) Cooling: 100 W m^{-2} (d) Cooling: 200 W m^{-2}

FIG. 3. As in Fig. 2, but with four different heat fluxes: −200, −100, 100, and 200 W m^{-2}. The dashed lines are the same as the lines plotted in Fig. 2.

compute J_z^B, J_z^W, and J_z^F, we need mixed layer depth, sea surface density, the air–sea heat and freshwater fluxes, and surface winds. All these variables are obtained from the HYCOM reanalysis dataset (Chassignet et al. 2007). We only show results from the year 2006, although none of our conclusions are sensitive to this choice. The surface wind is taken from the European Centre for Medium-Range Weather Forecasts (ECMWF) Interim Re-Analysis (ERA-Interim) dataset (Uppala et al. 2005) and interpolated on the HYCOM grid. We compute the stress according to the standard Large and Pond (1982) estimate,

$$\boldsymbol{\tau} = \rho_a C_d |\mathbf{u}_s| \mathbf{u}, \qquad (14)$$

where $\mathbf{u}$ is the surface wind; ρ_a is the density of air set to 1.3 kg m^{-3}; $|\mathbf{u}_s| = \max(|\mathbf{u}|, 1)$; and C_d is the drag (or exchange) coefficient given by the empirical law,

$$C_d = \frac{2.7 \times 10^{-3}}{|\mathbf{u}_s|} + 1.42 \times 10^{-4} + 7.64 \times 10^{-5} |\mathbf{u}_s|. \qquad (15)$$

Figure 4 corresponds to the components of the surface PV fluxes in January 2006 and July 2006, specifically J_z^B (top two rows), J_z^F (third row), and J_z^W (bottom row). The buoyancy contribution is separated into its two constituents: namely, that due to heat flux $Q_{\rm net}$ and that due to freshwater flux $E - P$. The scale is common in all plots, which has the effect of suppressing features in some of them.

In January, all contributions tend to extract PV. The buoyancy term (top panel) is maximum in the Gulf Stream area, whereas the wind mixing term (bottom panel) is maximum near St Johns. The contribution of J_z^F (third row) is at least one order of magnitude smaller than the other terms. We emphasize that the strength of the wind–front interaction is sensitive to resolution, so

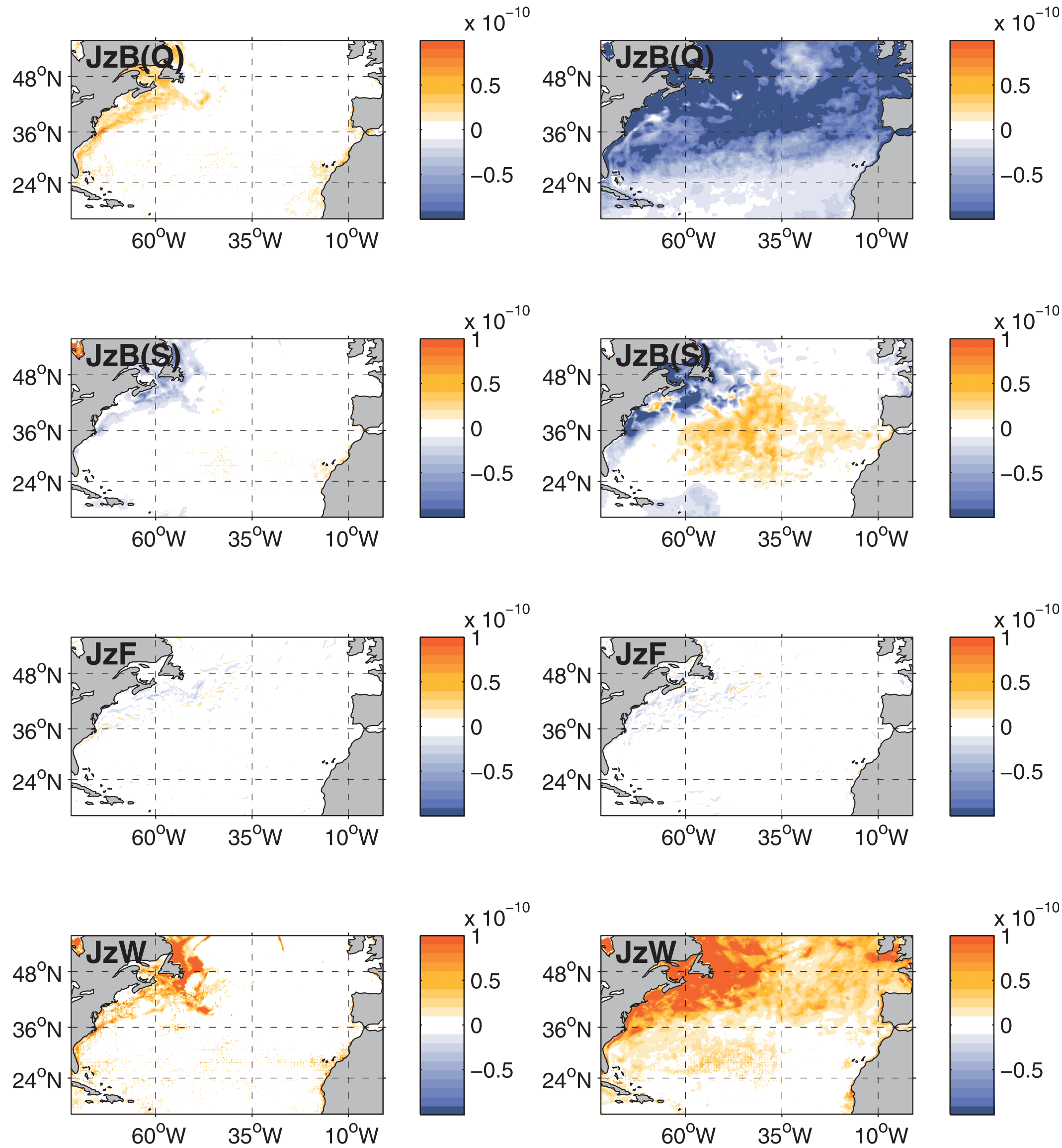

FIG. 4. Maps of monthly-mean values of the different components of the J_z vector: (top)–(bottom) the $Q_{\rm net}$ part of J_z^B, the $S_{\rm net}$ part of J_z^B, the Ekman component J_z^F, and the wind mixing term J_z^W. Values are for (left) January and (right) July. Units are kg m^{-3} s^{-2}.

that in regions of extremely sharp density gradients, like the Gulf Stream, we may underestimate it. On the other hand, sharpened gradients also limit the area over which down-front winds can generate PV, so the area average of the estimates should be quite insensitive. Note also that, over a large area of the Atlantic, the freshwater contribution $J_z^B(S)$ (the second row) is positive and thus decreases the PV. This is mainly due to the evaporation that occurs in the area.

In summer (Fig. 4, right), the sign of the heat flux is inverted and the resulting heat input restratifies the ocean. The summer pattern of $J_z^B(S)$ is comparable to winter but is now more pronounced. This is due to the drastically different summer mixed layer depths. Again J_z^F is a small contribution when comparing with the other maps. It is slightly negative in the Gulf Stream area. On the other hand, wind mixing PV destruction is pronounced. This effect is in fact more efficient in summer when the depth of the mixed layer is smaller than in winter, even allowing for the summertime reduction of entrainment. We see that this term is large over the entire northern part of the basin. The maximum remains confined in the western part of the Atlantic, where winds are the most intense and the mixed layer is the shallowest.

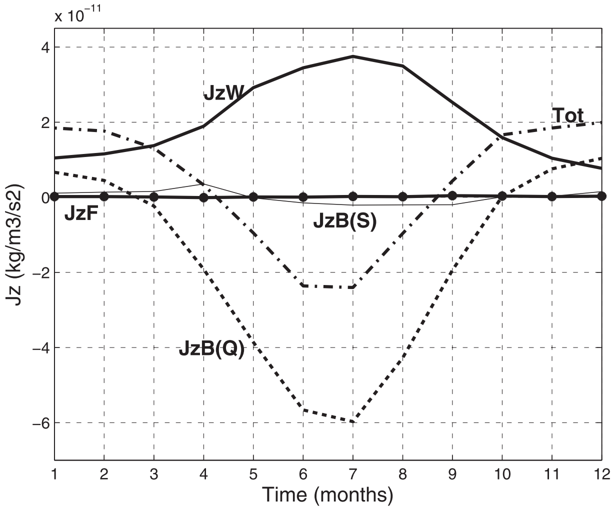

FIG. 5. Time series of the spatial mean computed over the domain shown in Fig. 4: J_z^W (solid thick line), $J_z^B(Q)$ (dashed thick line), J_z^F (solid thick line with bullets), $J_z^B(S)$ (solid thin line), and the sum of these four components (dashed–dotted thick line) during the year 2006.

The intermediate months (not shown) evolve smoothly between winter and summer. The quantity $J_z^B(Q)$ becomes positive in the Gulf Stream area in September. Its contribution to PV extraction is maximum in February and in April becomes negative again. The quantity J_z^F remains small all the year and is negative in the Gulf Stream area. The maps of J_z^W shown in Fig. 4 represent correctly the two extrema obtained in winter and in summer. We observe a constant increase over the entire basin from January to July and a constant decrease from July to January (this global tendency is verified in Fig. 5).

Water mass dynamics broadly speaking is sensitive to the integrated input of PV between density surfaces. Net inputs like this appear in Fig. 5, where the monthly-mean time series of each of the spatially averaged components of J_z appear. Because several averages are performed to produce these curves, caution should be exercised in any interpretation; however, the plot suffices to indicate the nature of the PV flux into the North Atlantic during a typical year.

As expected, J_z^W (thick solid line) is always positive (PV extracting). The wind always acts to deepen the mixed layer and has a greater intensity in the summer. The quantity $J_z^B(Q)$ (thick dashed line) exhibits the strongest seasonal cycle and often controls the net input. One observes the deepening/restratification of the mixed layer in winter/summer mainly because of this term. The spatial average of $J_z^B(S)$ (thin line) is harder to interpret because we saw in Fig. 4 that this term is not uniform over the Atlantic basin. Hence, the smallness of this term does not reflect the large values observed in Fig. 4. We see, however, that the global contribution of the freshwater flux is small compared to the net heat flux term and globally acts in the same way as $J_z^B(Q)$. The quantity J_z^F (line with bullets) remains close to zero throughout the year. The sum of all these terms is plotted using the thick dashed–dotted line. Extraction of PV mainly occurs in winter, whereas there is input of PV in the summer. The mean values of the terms J_z^W and $J_z^B(Q)$ (year integral) are 2×10^{-11} and -1.7×10^{-11} kg m^{-3} s^{-2}, respectively: that is, of the same order of magnitude.

5. Conclusions

a. Summary

Quantifying correctly the surface PV flux is of prime importance for understanding the formation of water masses and the dynamics of the ocean. In this study, we revisited the role played by wind in PV creation. It is known that Ekman currents induced by wind can destroy or create PV in regions of strong SST (or density) fronts (Thomas 2005). In contrast to this mechanical PV production, there are also diabatic consequences of winds that can affect PV budgets through a buoyancy mechanism. We here focus on the mixing induced by wind to evaluate the efficiency by which it generates PV.

Using a one-dimensional ocean mixed layer schematic (Fig. 1), we are able to derive a PV wind mixing scaling law,

$$J_z^W = \frac{0.7 f \rho u_*^3}{g h^2}. \tag{16}$$

Only the mixed layer depth h and the friction velocity u_* are needed to assess PV modification. This scaling is tested using an oceanic general circulation model. Comparing the scaling law with the PV flux obtained from primitive equation experiments under a variety of conditions suggests that it is a useful scaling of the extraction of PV due to wind (Fig. 2).

We also tested the validity of this scaling law when a heat flux is added to the wind (Fig. 3). It clearly appears that the wind effect is reduced if the ocean is heated. On the other hand, the wind effect is enhanced when the ocean is cooled. However, in both cases, $\lambda = 0.7$ remains a good approximation. For a better estimate of λ, one can still use the values mentioned in section 3c.

Finally, we used this scaling to compare wind mixing to the other mechanisms responsible for PV modification. Several maps are shown in winter and in summer (Fig. 4). PV extraction by this mechanism is more intense in summer when the mixed layer is shallow. Importantly, the magnitude of J_z^W is comparable to the size of heat flux contribution J_z^B in winter (Fig. 5), which is normally thought to control PV production.

b. Discussion

Equation (12) attempts to linearly relate entrainments to wind working. This is a strong assumption, but we found it is a skilled approximation (Fig. 2). However, the complexity of phenomenon occurring in the mixed layer motivates us to continue looking for refinements using LESs and observations. Refinement is especially needed when heat flux and wind stress are both acting on the mixed layer. In that case, we think that estimating λ as a function of ΔE [see Eq. (13)] would give more accurate results.

Also it is clear that, if ocean data are available at good spatial and temporal resolution, it is much better to compute the PV flux according to the raw formulation [Eq. (5)]. From our computation, it also appears that replacing λu_*^3 by $g'hdh/dt$ [Eq. (10)] in the scaling law [Eq. (12)] gives a very good estimate of the PV flux. We also noticed that, when the depth of the mixed layer varies rapidly (due to a sudden change of the wind stress), λu_*^3 always underestimates $g'hdh/dt$. In that case, J_z^W [computed with Eq. (12)] is a lower bound of the PV extraction. A possible fix is to modify λ in Eq. (10) so that it reflects wind history; for example, $\lambda = \lambda_0 + \lambda_1[u(t) - u(t - T)]$, where $u(t)$ is the wind strength at time t and T is a time constant. More generally, the link between PV extraction and the wind might help to dynamically connect Atlantic weather regimes (e.g., the North Atlantic Oscillation) with mode water formation (Joyce et al. 2000).

Acknowledgments. Comments from two anonymous reviewers greatly improved this manuscript, and we are particularly indebted to *JPO* Editor Jerome Smith for his professional handling of our manuscript. This work was supported by NSF Grant OCE-0960500.

REFERENCES

Agrawal, Y. C., E. A. Terray, M. A. Donelan, P. A. Hwang, A. J. Williams III, W. M. Drennan, K. K. Kahma, and S. A. Krtaigorodskii, 1992: Enhanced dissipation of kinetic energy beneath surface waves. *Nature,* **359,** 219–220, doi:10.1038/359219a0.

Alford, M. H., 2003a: Improved global maps and 54-year history of wind-work on ocean inertial motions. *Geophys. Res. Lett.,* **30,** 1424, doi:10.1029/2002GL016614.

——, 2003b: Redistribution of energy available for ocean mixing by long-range propagation of internal waves. *Nature,* **423,** 159–162, doi:10.1038/nature01628.

Bernie, D. J., S. J. Woolnough, J. M. Slingo, and E. Guilyardi, 2005: Modeling diurnal and intraseasonal variability of the ocean mixed layer. *J. Climate,* **18,** 1190–1202.

Chassignet, E. P., H. E. Hurlburt, O. M. Smedstad, G. R. Halliwell, P. J. Hogan, A. J. Wallcraft, R. Baraille, and R. Bleck, 2007: The HYCOM (HYbrid Coordinate Ocean Model) data assimilative system. *J. Mar. Syst.,* **65,** 60–83, doi:10.1016/j.jmarsys.2005.09.016.

Cushman-Roisin, B., 1981: Deepening of the wind-mixed layer: A model of the vertical structure. *Tellus,* **33,** 564–582.

Czaja, A., and U. Hausmann, 2009: Observations of entry and exit of potential vorticity at the sea surface. *J. Phys. Oceanogr.,* **39,** 2280–2294.

D'Asaro, E. A., 2001: Turbulent vertical kinetic energy in the ocean mixed layer. *J. Phys. Oceanogr.,* **31,** 3530–3537.

——, C. Lee, L. Rainville, R. Harcourt, and L. Thomas, 2011: Enhanced turbulence and energy dissipation at ocean fronts. *Science,* **332,** doi:10.1126/science.1201515.

De Szoeke, S. P., and P. B. Rhines, 1976: Asymptotic regimes in mixed-layer deepening. *J. Mar. Res.,* **34,** 111–116.

Durski, S. M., S. M. Glenn, and D. B. Haidvogel, 2004: Vertical mixing schemes in the coastal ocean: Comparison of the level 2.5 Mellor-Yamada scheme with an enhanced version of the K profile parameterization. *J. Geophys. Res.,* **109,** C01015, doi:10.1029/2002JC001702.

Gerbi, G. P., J. H. Trowbridge, E. A. Terray, A. J. Plueddemann, and T. Kukulka, 2009: Observations of turbulence in the ocean surface boundary layer: Energetics and transport. *J. Phys. Oceanogr.,* **39,** 1077–1096.

Grant, A. L. M., and S. E. Belcher, 2011: Wind-driven mixing below the oceanic mixed layer. *J. Phys. Oceanogr.,* **41,** 1556–1575.

Hanawa, K., and L. D. Talley, 2001: Mode waters. *Ocean Circulation and Climate: Observing and Modelling the Global Ocean,* G. Siedler, J. Church, and J. Gould, Eds., International Geophysics Series, Vol. 77, Academic Press, 373–386.

Harcourt, R. R., and E. A. D'Asaro, 2008: Large-eddy simulation of Langmuir turbulence in pure wind seas. *J. Phys. Oceanogr.,* **38,** 1542–1562.

Haynes, P. H., and M. E. McIntyre, 1987: On the evolution of vorticity and potential vorticity in the presence of diabatic heating and frictional or other forces. *J. Atmos. Sci.,* **44,** 828–841.

Joyce, T. M., C. Deser, and M. A. Spall, 2000: The relation between decadal variability of subtropical mode water and the North Atlantic Oscillation. *J. Climate,* **13,** 2550–2569.

Kara, A. B., P. A. Rochford, and H. E. Hurlburt, 2000: Mixed layer depth variability and barrier layer formation over the North Pacific Ocean. *J. Geophys. Res.,* **105,** 16 783–16 802.

Large, W. G., and S. Pond, 1982: Sensible and latent heat flux measurements over the ocean. *J. Phys. Oceanogr.,* **12,** 464–482.

——, and P. R. Gent, 1999: Validation of vertical mixing in an equatorial ocean model using large eddy simulations and observations. *J. Phys. Oceanogr.,* **29,** 449–464.

——, J. C. McWilliams, and S. C. Doney, 1994: Oceanic vertical mixing: A review and a model with a nonlocal boundary layer parameterization. *Rev. Geophys.,* **32,** 363–404.

Li, M., C. Garrett, and E. Skyllingstad, 2005: A regime diagram for classifying turbulent large eddies in the upper ocean. *Deep-Sea Res. I,* **52,** 259–278, doi:10.1016/j.dsr.2004.09.004.

Li, X., Y. Chao, J. C. McWilliams, and L.-L. Fu, 2001: A comparison of two vertical-mixing schemes in a Pacific Ocean general circulation model. *J. Climate,* **14,** 1377–1398.

Marshall, J. C., and A. J. G. Nurser, 1992: Fluid dynamics of oceanic thermocline ventilation. *J. Phys. Oceanogr.,* **22,** 583–595.

——, ——, and R. G. Williams, 1993: Inferring the subduction rate and period over the North Atlantic. *J. Phys. Oceanogr.,* **23,** 1315–1329.

——, A. Adcroft, C. Hill, L. Perelman, and C. Heisey, 1997: A finite-volume, incompressible Navier Stokes model for studies of the ocean on parallel computers. *J. Geophys. Res.,* **102,** 5753–5766.

——, D. Jamous, and J. Nilsson, 2001: Entry, flux, and exit of potential vorticity in ocean circulation. *J. Phys. Oceanogr.,* **31,** 777–789.

Marshall, J. C., and Coauthors, 2009: The Climode field campaign: Observing the cycle of convection and restratification over the Gulf Stream. *Bull. Amer. Meteor. Soc.,* **90,** 1337–1350.

McDowell, S., P. Rhines, and T. Keffer, 1982: North Atlantic potential vorticity and its relation to the general circulation. *J. Phys. Oceanogr.,* **12,** 1417–1436.

McWilliams, J. C., and P. P. Sullivan, 2000: Vertical mixing by Langmuir circulations. *Spill Sci. Technol. Bull.,* **6** (3–4), 225–237.

——, ——, and C.-H. Moeng, 1997: Langmuir turbulence in the ocean. *J. Fluid Mech.,* **334,** 1–30.

Niiler, P. P., and E. B. Krauss, 1977: One-dimensional models of the upper ocean. *Modeling and Prediction of the Upper Layers of the Ocean,* E. B. Krauss, Ed., Pergamon Press, 143–172.

Pedlosky, J., 1996: *Ocean Circulation Theory*. Springer-Verlag, 453 pp.

Pollard, R. T., P. B. Rhines, and R. O. R. Y. Thompson, 1972: The deepening of the wind-mixed layer. *Geophys. Fluid Dyn.,* **4,** 381–404, doi:10.1080/03091927208236105.

Price, J. F., R. A. Weller, and R. Pinkel, 1986: Diurnal cycling: Observations and models of the upper ocean response to diurnal heating, cooling, and wind mixing. *J. Geophys. Res.,* **91,** 8411–8427.

Rintoul, S. R., and M. H. England, 2002: Ekman transport dominates local air–sea fluxes in driving variability of Subantarctic Mode Water. *J. Phys. Oceanogr.,* **32,** 1308–1321.

Skyllingstad, E. D., and D. W. Denbo, 1995: An ocean large-eddy simulation of Langmuir circulations and convection in the surface mixed layer. *J. Geophys. Res.,* **100,** 8501–8522.

——, W. D. Smyth, and G. B. Crawford, 2000: Resonant wind-driven mixing in the ocean boundary layer. *J. Phys. Oceanogr.,* **30,** 1866–1890.

Smith, J. A., 1998: Evolution of Langmuir circulation during a storm. *J. Geophys. Res.,* **103,** 12 649–12 668.

——, 2001: Observations and theories of Langmuir circulation: A story of mixing. *Fluid Mechanics and the Environment: Dynamical Approaches,* J. L. Lumley, Ed., Lecture Notes in Physics, Vol. 566, Springer-Verlag, 295–314.

Smyth, W. D., E. D. Skyllingstad, G. B. Crawford, and H. Wijesekera, 2002: Nonlocal fluxes and Stokes drift effects in the K-profile parameterization. *Ocean Dyn.,* **52,** 104–115, doi:10.1007/s10236-002-0012-9.

Sullivan, P. P., and J. C. McWilliams, 2010: Dynamics of winds and currents coupled to surface waves. *Annu. Rev. Fluid Mech.,* **42,** 19–42, doi:10.1146/annurev-fluid-121108-145541.

Talley, L. D., and M. E. Raymer, 1982: Eighteen Degree Water variability. *J. Mar. Res.,* **40,** 757–775.

Terray, E. A., M. A. Donelan, Y. C. Agrawal, W. M. Drennan, K. K. Kahma, A. J. Williams, P. A. Hwang, and S. A. Kitaigorodskii, 1996: Estimates of kinetic energy dissipation under breaking waves. *J. Phys. Oceanogr.,* **26,** 792–807.

Thomas, L. N., 2005: Destruction of potential vorticity by winds. *J. Phys. Oceanogr.,* **35,** 2457–2466.

Thorpe, S. A., 2004: Langmuir circulation. *Annu. Rev. Fluid Mech.,* **36,** 55–79, doi:10.1146/annurev.fluid.36.052203.071431.

——, T. R. Osborn, J. F. E. Jackson, A. J. Hall, and R. G. Lueck, 2003: Measurements of turbulence in the upper-ocean mixing layer using autosub. *J. Phys. Oceanogr.,* **33,** 122–145.

Uppala, S. M., and Coauthors, 2005: The ERA-40 Re-Analysis. *Quart. J. Roy. Meteor. Soc.,* **131,** 2961–3012.

Warren, B. A., 1972: Insensitivity of subtropical mode water characteristics to meteorological fluctuations. *Deep-Sea Res. Oceanogr. Abstr.,* **19,** 1–19, doi:10.1016/0011-7471(72)90069-1.

Wijesekera, H. W., J. S. Allen, and P. A. Newberger, 2003: Modeling study of turbulent mixing over the continental shelf: Comparison of turbulent closure schemes. *J. Geophys. Res.,* **108,** 3103, doi:10.1029/2001JC001234.

Wunsch, C., and R. Ferrari, 2004: Vertical mixing, energy, and the general circulation of the oceans. *Annu. Rev. Fluid Mech.,* **36,** 281–314, doi:10.1146/annurev.fluid.36.050802.122121.